


Rotational-state-selective field ionization of H₂ Rydberg states

William J. Setzer^{*,} Alexander de Magalhaes,[†] and Thomas J. Morgan
Department of Physics, Wesleyan University, Middletown, Connecticut 06459, USA

 (Received 2 August 2019; published 17 January 2020)

This paper presents rotational-state-selective field-ionization spectra of highly excited triplet nd H₂ Rydberg states. A fast 6 keV beam of metastable $c^3\Pi_u^- 2p\pi$ molecules is excited to $v = 0, N^+ = 1$ Rydberg states ($n = 17$ to 27) by a frequency-doubled tunable dye laser and ionized by static electric fields. The resulting measured total ionization yields are analyzed using a model that considers a diabatic ionization pathway through the Stark map. A field of up to ~ 4 kV cm⁻¹ mixes Stark manifolds, while a field of up to ~ 36 kV cm⁻¹ ionizes the resulting mixture. Rotational-state population transfer of up to 50% is observed, populating neighboring $N^+ = 3$ manifolds ($n = 12$ to $n = 16$). Control over the rotational quantum state composition of the field-ionized molecules is demonstrated.

DOI: [10.1103/PhysRevA.101.013425](https://doi.org/10.1103/PhysRevA.101.013425)

I. INTRODUCTION

In selective field ionization (SFI), an external field is applied to an atom or molecule and ramped, leading to ionization. Different Rydberg states of atoms and molecules ionize at different fields, and therefore it is possible to identify them by their field-ionization signal. In this way, SFI has been exploited as an experimental tool to measure the character and population of Rydberg states.

The field strength at which a particular Rydberg state ionizes depends on the ionization mechanism, which, in turn, depends on the rate at which the field is ramped. This rate is known as the slew rate. Numerous experiments have been performed to investigate ionization mechanisms in atoms [1–5]. Shaped pulses have been shown to improve selectivity in SFI by manipulating the ionization pathway [4,5]. In atomic SFI experiments nS states have been diabatically transferred into a product state consisting of high- l states of a neighboring Stark manifold. An experiment by Zhang *et al.* demonstrates that this transfer can be manipulated and that the population of the product state increases with amplitude and hold time of the pulse [6].

The dynamics of SFI of molecular Rydberg states have been investigated to a lesser extent. Patel *et al.* investigated SFI dynamics in NO, where it was shown that the slew rate of a linearly ramped electric field can be exploited to control the rotational quantum state composition of field-ionized molecules [7]. Rotational population transfer has also been observed in field-induced rotational autoionization [8–11] and in ionization at a metal surface [12]. The field-ionization properties of a fast H₂ beam traversing static electric fields have also been studied [13].

In the present work, a different experimental approach is taken. A time-dependent electric field is not generated

in the conventional way, where a voltage is varied in time affecting stationary molecules in a uniform field. Instead, a fixed voltage is applied between electrodes to define a nonuniform field in space. Fast molecules traverse that space resulting in a time-dependent electric field experienced by the molecules. In this way, we investigate the SFI of well-defined laser excited H₂ Rydberg states using a shaped pulse, with high slew rates and high field strengths, generated by a fast molecular Rydberg beam traversing two static field regions. The amplitude of the shaped pulse manipulates the ionization pathway, through electron-nuclear coupling, allowing for control over the rotational quantum state composition of the field-ionized molecules.

When an external field is applied to a Rydberg atom or molecule, the spherical symmetry of the Rydberg system is broken and the orbital angular momentum quantum number l is no longer good. At high n , the Stark states of atoms and molecules can be approximated by atomic hydrogen. In atomic hydrogen, the Schrödinger equation is separable in parabolic coordinates. The eigenfunctions are characterized by the parabolic quantum numbers n_1 and n_2 , and the orbital magnetic quantum number m [14]. The principal quantum number n is

$$n = n_1 + n_2 + |m| + 1. \quad (1)$$

The energies of the Stark eigenstates, given from first-order perturbation theory in atomic units, are

$$E_{\text{Stark}} = -1/2n^2 + 3/2nkF, \\ k = n_1 - n_2. \quad (2)$$

In atomic hydrogen, the eigenstates of a single n , which are degenerate at zero field, fan out linearly with field strength until they cross Stark states of neighboring n manifolds at the Inglis-Teller limit, $F = 1/3n^5$. In nonhydrogenic atoms or molecules, the zero field degeneracy is lifted. The Stark states are coupled due to the finite size of the ion core and form multilevel avoided crossings. The probability of a diabatic transition is given by the well-known Landau-Zener

*Present address: Sandia National Laboratories, 315 Narcissus, Pl SE Albuquerque, NM 87123, Mexico; wjsetze@sandia.gov

†Present address: Machine Learning Engineer, Quantiphi, Inc., 256 Edmands Road, Framingham, MA 01701, USA.

formula [15],

$$P_{\text{diabatic}} = \exp \left[\frac{-2\pi |V_{ij}|^2}{\hbar dW_{ij}/dt} \right], \quad (3)$$

where V_{ij} is the coupling matrix of interaction, which relates to the energy separation between the Stark states at their crossing by $W_{ij} = 2V_{ij}$. The rate of change of the energy separation is

$$dW_{ij}/dt = |dE_i/dF - dE_j/dF| |dF/dt|,$$

where dF/dt is the slew rate of the electric field applied. For low slew rates, such that $P_{\text{diabatic}} \approx 0$, the crossings in the Stark map are traversed adiabatically. An adiabatic traverse of the Stark map leads to a sawtoothlike trajectory, at a nearly constant energy, until ionization at the classical saddle point, $F_s = 1/16n^4$. For high slew rates, such that $P_{\text{diabatic}} \approx 1$, the crossings are traversed diabatically and the trajectory through the Stark map will be hydrogenic.

The addition of an external electric field to the Coulomb potential of the atom or molecule creates a saddle point at $E_s = -2\sqrt{F}$. Red Stark states have charge distributions localized near this saddle point, whereas blue Stark states are localized on the other side of the potential well. As a result, in diabatic ionization, the field-ionization rate must be considered and ionization begins with the reddest Stark state (most negative k) at $F_{\text{red}} = 1/9n^4$ and ends with the bluest Stark state (most positive k) at approximately twice that field, $F_{\text{blue}} \approx 2F_{\text{red}}$. For a Stark state with quantum numbers n , n_1 , n_2 , and m , the approximate field-ionization rate for atomic hydrogen is given by [16]

$$\Gamma = \frac{4R^{2n_2+m+1}}{n^3 n_2! (n_2 + m)!} \exp \left[\frac{-2R}{3} - \frac{n^3 F}{4} \left(34n_2^2 + 34n_2 m + 46n_2 + 7m^2 + 23m + \frac{53}{3} \right) \right], \quad (4)$$

$$R = \frac{-2E_{\text{Stark}}^{3/2}}{F}.$$

For a given ionization rate, Eq. (4) can be solved numerically to determine the field strength required to ionize a given Rydberg state. In the present experiment, the static electric-field geometry along with the speed of the Rydberg beam result in an ionizing field with an ~ 2 ns peak duration. Our experimental setup requires that ionization occurs early within this field for detection. Therefore, we expect an observable ionization rate on the order of $\sim 10^{10} \text{ s}^{-1}$.

II. EXPERIMENT

The experimental setup has been described in detail in a previous work [17]. Briefly, a 6 keV H_2^+ ion beam is produced by a Colutron ion source [18]. This ion beam is neutralized by a potassium vapor cell resulting in a beam of metastable $c^3\Pi_u^- 2p\pi$ molecules. The metastable beam serves as the initial state for the experiment and is excited in an ~ 30 cm field-free interaction region by a counterpropagating UV laser beam. The ~ 340 nm UV photon required for excitation is generated by a laser system consisting of a 20 Hz, ~ 10 ns, 532 nm, Quanta Ray Nd-YAG laser pumping a frequency-

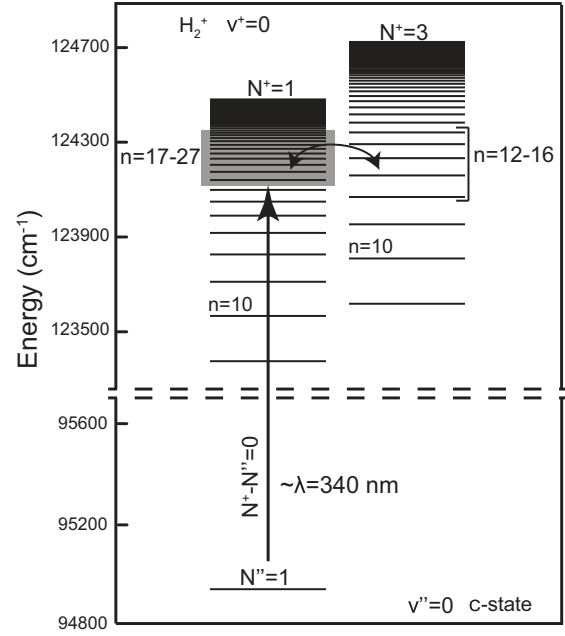


FIG. 1. Energy-level diagram of triplet nd Rydberg states. The diagram illustrates Rydberg series converging to the $v^+ = 0$, $N^+ = 1$, and $N^+ = 3$ rovibronic states of the molecular ion. The $N^+ = 1$ states shaded in gray are excited in the present work. Coupling between the series is indicated. Energies are listed in cm^{-1} with respect to ground state H_2 .

doubled Lambda Physik ScanMate tunable dye laser. Figure 1 shows an energy-level diagram depicting the excitation to the Rydberg states studied ($v = 0$, $N^+ = 1$, $n = 17$ to 27), as well as the neighboring $N^+ = 3$ states ($v = 0$, $N^+ = 3$, $n = 12$ to 16). H_2 triplet Rydberg states have been investigated in detail, and the spectroscopic properties of these states are well characterized [17,19–24]. To illustrate the proximity of the neighboring Stark manifolds, a first-order hydrogenic approximation of the molecular Stark map is shown in Fig. 2.

A schematic of the interaction and detection experimental setup is shown in Fig. 3. After excitation in the field-free interaction region the Rydberg beam propagates through two electric-field regions referred to collectively as the “field ionizer.” The field ionizer consists of three highly polished stainless steel electrodes with 1.5 mm apertures spaced 2 cm and 2 mm apart. The two outer electrodes are grounded, and a voltage (V) ranging from 0 to 8 kV is applied to the center electrode. The electrode spacing and applied voltage create two static electric-field regions: a weak mixing field (0 to $\sim 4 \text{ kV cm}^{-1}$) and a strong ionizing field (0 to $\sim 36 \text{ kV cm}^{-1}$).

Figure 4 shows the field strength and slew rate that results when the 6 keV Rydberg beam passes through the field ionizer ($V = 2 \text{ kV}$). The apertures limit the maximum field strength of the ionizing field region to $\sim 90\%$ of an ideal parallel plate capacitor. Therefore, 8 kV applied to the center electrode results in ionizing field strengths of up to $\sim 36 \text{ kV cm}^{-1}$. In our experiment, the field ionizer serves two purposes: to kinetic energy separate field-ionizing ions from autoionizing ions and to manipulate the ionization pathway. We discuss the former below, and the latter will be discussed in the Results and Discussion section.

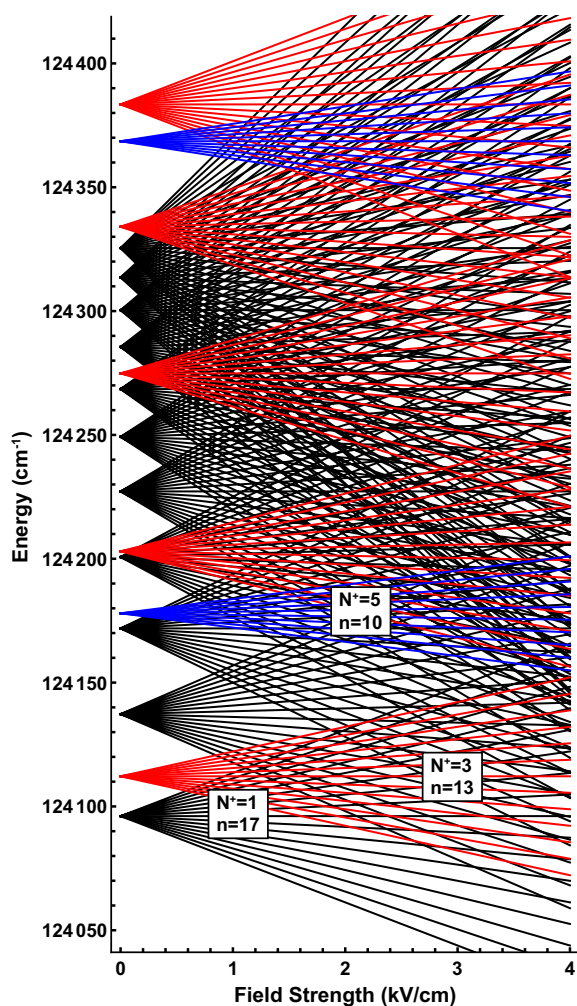


FIG. 2. First-order hydrogenic Stark map ($m = 0$), for the $v = 0$, odd N^+ , states of H_2 . The diagram illustrates the proximity of neighboring interacting Stark manifolds: $N^+ = 1$, $n = 17-27$ (black); $N^+ = 3$, $n = 13-17$ (red); $N^+ = 5$, $n = 10$ and 11 (blue).

The kinetic-energy separation requires that the mixing field strength not field ionize the bound Rydberg states of interest. First, the mixing field decelerates autoionizing Rydberg states,

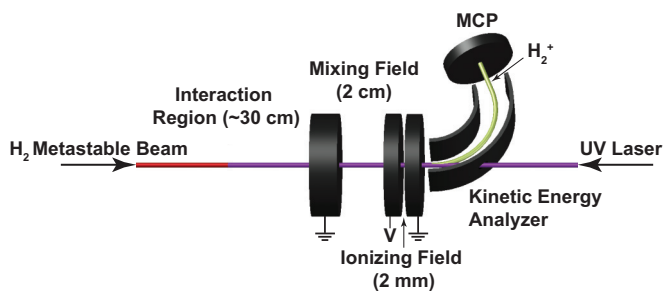


FIG. 3. Schematic of the apparatus. A 6 keV metastable molecular beam is excited in the ~ 30 cm field-free interaction region by a counterpropagating UV laser beam. The resulting Rydberg molecules ionize within the ionizing field region of the field ionizer. The resulting H_2^+ ions are deflected by the steering plates of the kinetic-energy analyzer and detected by the microchannel plate (MCP).

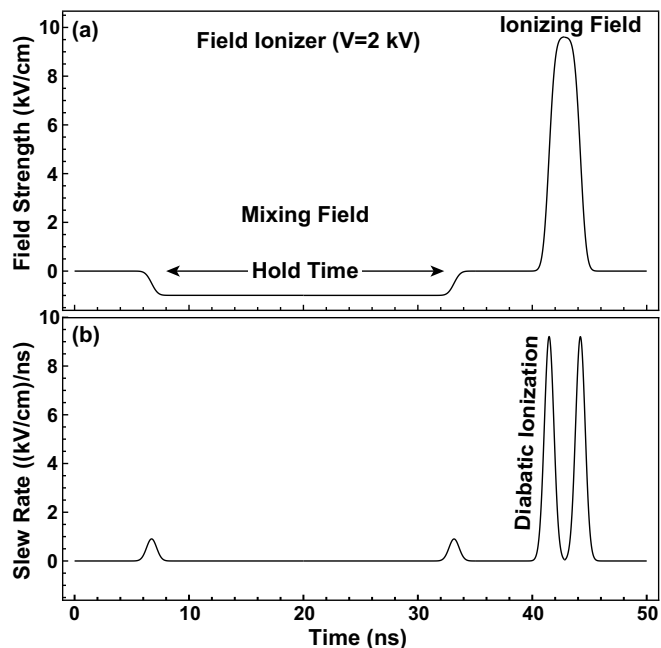


FIG. 4. (a) Idealized shaped pulse felt by the 6 keV Rydberg molecules as they pass through the static electric fields of the ionizer. The static field along the beam axis is modeled using finite element analysis for 2 kV placed on the center electrode of the field ionizer. The electrode configuration results in two field regions. The ionizing field differs in polarity from the mixing field and is ~ 9 times stronger. (b) The slew rate of the shaped pulse ($|dF/dt|$). The pulse has a high slew rate except during passage through the electrodes near zero field and during ~ 24 ns traverse of the mixing field region.

separating them in kinetic energy from the bound Rydberg states. Second, the ionizing field ionizes the bound Rydberg states, accelerating them. Two curved steering plates spaced 1 cm apart are used to analyze the kinetic energy of the H_2^+ ions detected by a microchannel plate (MCP).

Figure 5 shows a kinetic-energy map of detected H_2^+ ions resulting from the field ionization of $N^+ = 1$, $n = 22$. For several voltages placed on the center electrode of the field ionizer, the voltage placed on the inner deflector plate of the kinetic-energy analyzer is scanned to detect ions with kinetic energies up to 14 keV. The ion yield with kinetic energy 6 keV results from autoionization. The H_2^+ beam is nearly monoenergetic. Therefore, the detected kinetic-energy width of the autoionized ion yield is due to the range of the voltages placed on the kinetic-energy analyzer for which ion trajectories are incident on the detector face. This width is defined by the 1 cm spacing between the deflector plates. The autoionization yield is present until ~ 6 keV is placed on the center electrode of the field ionizer. At this voltage, the mixing field decelerates the incoming 6 keV ions until they are no longer detected. The small 3 keV ion yield at zero field results from dissociative ionization. This yield can be greatly enhanced by increasing the laser intensity, suggesting it results from multiphoton excitation. The ion yields with kinetic energies larger than 6 keV result from the field-ionized Rydberg state of interest. These ions arrive at the detector with kinetic energy equal to the 6 keV beam plus the kinetic energy

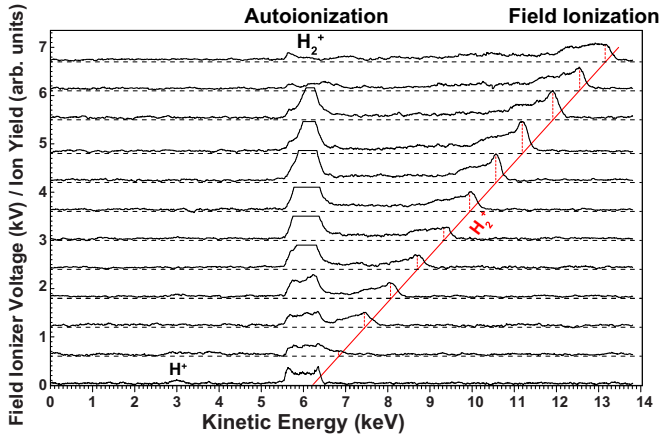


FIG. 5. Kinetic-energy map for $N^+ = 1$, $n = 22$. The $n = 22$ field-ionized Rydberg states (right) arrive with a kinetic-energy boost corresponding to the voltage placed on the center electrode of the field ionizer. The autoionizing states arrive with the kinetic energy of the beam (6 keV). At zero field, there is a small 3 keV peak resulting from dissociative ionization. The maximum field-ionized ion yield for a given voltage placed on the field ionizer is indicated by the red line.

gained from the ionizing field of the field ionizer. The red line indicates the maximum ion yield for each voltage placed on the field ionizer.

Recently, we have investigated the field-ionization spectroscopy of bound triplet H_2 Rydberg states in detail [17]. In Fig. 6, we show two field-ionization spectra in the same spectral region, investigated with ionizing fields of 4.5 kV cm^{-1} (blue) and 14.85 kV cm^{-1} (red). The amplitudes of the two spectra clearly differ. The $N^+ = 1$ Rydberg series is indicated by vertical dashed lines. The reduced ion yield at low n in the 4.5 kV cm^{-1} spectrum results from the ionizing field having

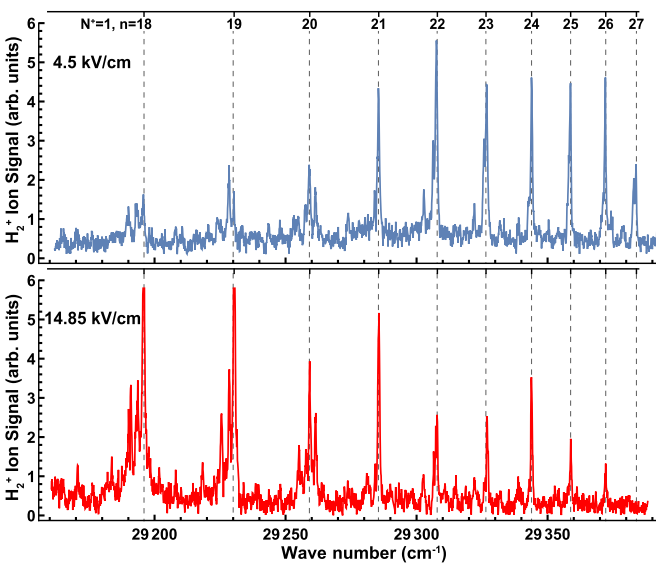


FIG. 6. Field-ionized triplet nd Rydberg spectra. Two field-ionized spectra, a 4.5 kV cm^{-1} (blue) and a 14.85 kV cm^{-1} (red), are shown for comparison. The $\nu = 0$, $N^+ = 1$ Rydberg series is indicated in the range $n = 18$ – 27 .

insufficient strength for ionization. The complete loss of ion yield for $n = 27$ in the 14.85 kV cm^{-1} spectrum is explained by ionization in the mixing field of the ionizer, resulting in ions that are not kinetic energy separated and hence are not detected.

III. RESULTS AND DISCUSSION

For each Rydberg state excited, a total ionization yield is measured. The laser is parked on the desired Rydberg state, and the voltage placed on the center electrode of the field ionizer is incremented from 0 to 8 kV. Simultaneously, the voltage difference between the deflector plates of the kinetic-energy analyzer is varied, along the red line of Fig. 5, to collect the resulting ions. The laser power and metastable beam current are carefully monitored during data acquisition and held constant within 10%. The voltage of the field ionizer is increased in 1 V increments, and ~ 5 laser shots are taken at each voltage.

The ion yields for excitation to $N^+ = 1$, $n = 17$ – 27 are shown in Fig. 7. To compare the ion yields of states with different transition probabilities, the yields are normalized, and a 100 point moving average is applied for smoothing. The onset of diabatic field ionization occurs at the reddest Stark state passes the saddle-point energy at $F_{\text{red}} = 1/(9n^4)$. For the $N^+ = 1$ Rydberg states, this is indicated by the first dashed black curve. The yield saturates when the bluest Stark state is ionized at approximately $2F_{\text{red}}$, indicated by the second dashed black curve.

At larger fields, a second increase in the ion yield is observed, as indicated by the first red dashed curve. We attribute this increase in yield to ionization of neighboring $N^+ = 3$ Rydberg states with lower principal quantum numbers, $n = 12$ – 16 , which have been populated by the mixing field. The onset of this yield also follows $F_{\text{red}} = 1/9n^4$, where n is the principal quantum number of the neighboring $N^+ = 3$ Rydberg state. The second dashed red curve indicates approximately $2F_{\text{red}}$.

For high voltages on the field ionizer, the mixing field reaches field strengths strong enough to ionize $N^+ = 1$ Rydberg states. The resulting ions are not detected, and a decrease in signal is observed. Ionization of the bluest and reddest Stark states by the mixing field is indicated by the green dashed curves.

In Fig. 8, a near degeneracy of $\sim 2 \text{ cm}^{-1}$ between the $N^+ = 1$ and $N^+ = 3$ series is examined. The field-ionization yield for excitation to the $N^+ = 1$, $n = 20$ Rydberg state is shown in Fig. 8(b). The ionization yield detected is a total ionization yield. Therefore, the derivative of this yield gives the ionization yield at individual field strengths. The experimental yield was fit piecewise using two error functions, and the derivative of this fit is shown in Fig. 8(c). Stark states are shown in Fig. 8(a) using the hydrogenic first-order Stark effect calculated with Eq. (2) ($m = 0$).

The $N^+ = 1$, $n = 20$ state (black) is nearly degenerate with the $N^+ = 3$, $n = 14$ (red). Because of this near degeneracy, low voltages placed on the ionizer mix the Stark states of the two manifolds. During ionization the Stark map is traversed diabatically due to the high slew rate of the field [Eq. (3) and Fig. 4]. In Fig. 8(a), the saddle-point energy, $E_s = -2\sqrt{F}$, is plotted for the $N^+ = 1$ and $N^+ = 3$ ionization limits, which

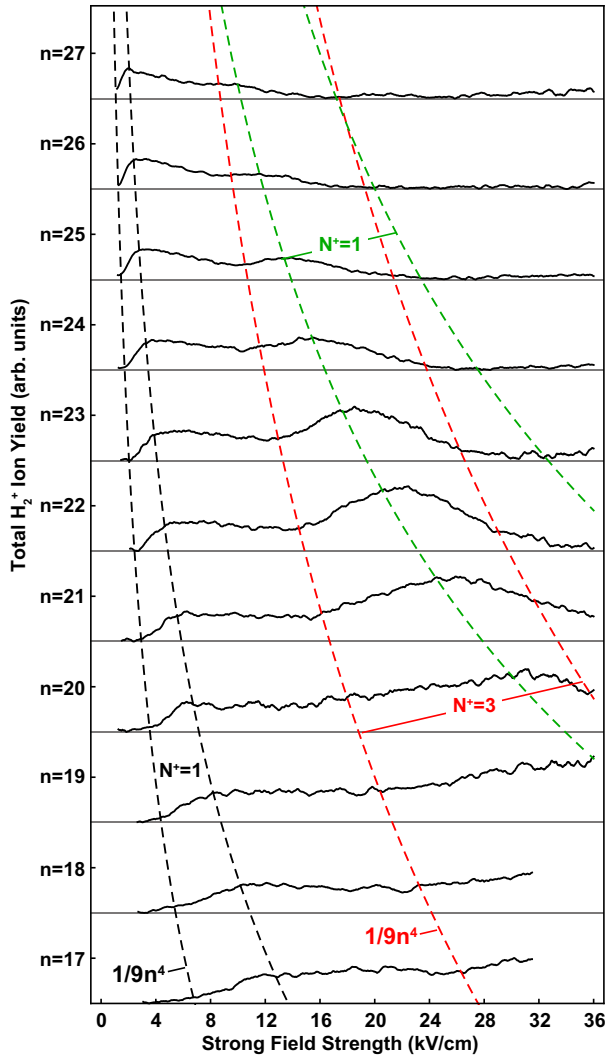


FIG. 7. Field-ionization yields for excitation to $N^+ = 1$, $n = 17$ – 27 . The excitation laser is parked on a particular n in the range $n = 17$ – 27 of the $N^+ = 1$ Rydberg series, and an ion yield is recorded. Two field-ionization regions are identified corresponding to the $N^+ = 1$ (black dashed curves) and $N^+ = 3$ (red dashed curves) states of the H_2^+ . At high voltages on the field ionizer, the mixing field is strong enough to ionize $N^+ = 1$ Rydberg states and a decrease in signal is observed (green dashed curves).

are separated by 288.45 cm^{-1} [25,26]. The ionizing field strength required for an observable ionization rate of 10^{10} s^{-1} is approximated by Eq. (4) and indicated by blue dots for each manifold. The red Stark states ($k < 0$), localized near the saddle point, ionize soon after crossing E_s . The blue Stark states ($k > 0$), localized opposite the saddle point, require higher fields to ionize at the same ionization rate. The behavior of the ion yield is consistent with the hydrogenic model (indicated by dashed lines).

Throughout the experiment, the voltage placed on the center electrode of the ionizer manipulates the ionization pathway in the Stark map. This voltage determines the amplitude of the shaped pulse (Fig. 4). The excited nd Rydberg states have small quantum defects $\sim \delta = 0.02$ and in the passage from zero field to the mixing field are projected onto Stark states of

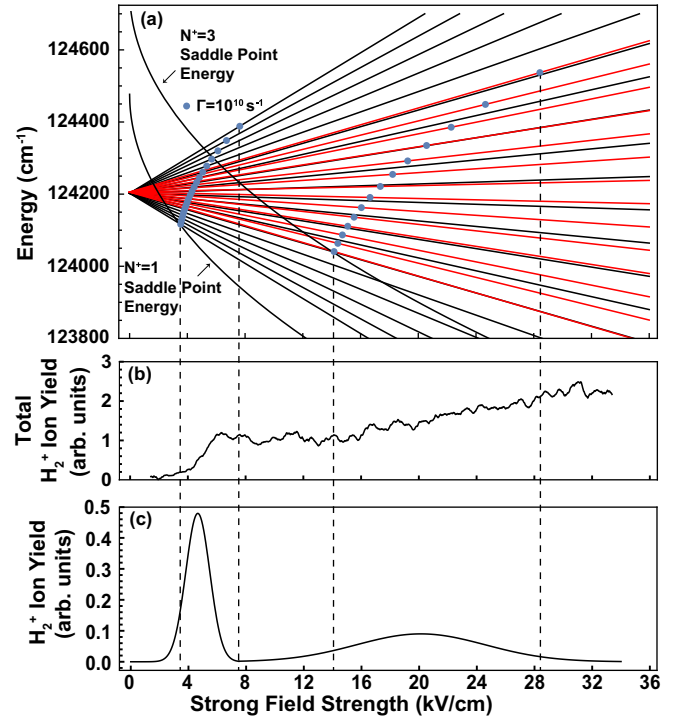


FIG. 8. Stark energy diagrams and field-ionization yield for laser excitation to $N^+ = 1$, $n = 20$. (a) Stark energy diagram for the $N^+ = 1$, $n = 20$ (black) and nearly degenerate $N^+ = 3$, $n = 14$ (red). The hydrogenic first-order $m = 0$ Stark states are shown. Ionization at a constant rate of 10^{10} s^{-1} is calculated for each Stark state by the ionization rate approximation for atomic hydrogen, as shown in Eq. (4) and is indicated by blue dots. (b) Measured total field-ionization yield for excitation to $N^+ = 1$, $n = 20$ (black). (c) The derivative of an error function fit to the experimental yield shows ionization yield at each field strength. Ion yield resulting from ionization of $N^+ = 1$ and $N^+ = 3$ Rydberg states is consistent with the hydrogenic model (black dashed lines).

their adjacent manifolds [17]. As $N^+ = 1$ Rydberg molecules enter the mixing field, the $N^+ = 1$ Stark manifold is diabatically traversed to the maximum mixing field strength. Here, the traverse of the map is halted during the $\sim 24 \text{ ns}$ hold time, and the composite nd and populated Stark states time evolve. During this holding time, dephasing accumulates [6]. As the Rydberg molecules exit the mixing field, the resulting state composition diabatically traverses back to a near zero field for $\sim 6 \text{ ns}$ before entering the ionizing field. When the Rydberg molecules enter the ionizing field region, each populated Stark manifold diabatically traverses the Stark map. The ionizing field strength then determines which Stark states are ionized, resulting in the total ionization yield detected.

In Fig. 9, a more complicated total ion yield is examined. Figure 9(a) shows the total ionization yield measured for excitation to the $N^+ = 1$, $n = 25$ Rydberg state (black). The yield is divided into four regions. The behavior of the yield in these regions is explained by manipulation of the Stark pathway shown in the mixing field [Fig. 9(b)] and the ionizing field [Fig. 9(c)]. In region A, no mixing occurs in the mixing field because the $N^+ = 3$ manifolds do not cross the $N^+ = 1$ manifold. The ionizing field reaches the ionization

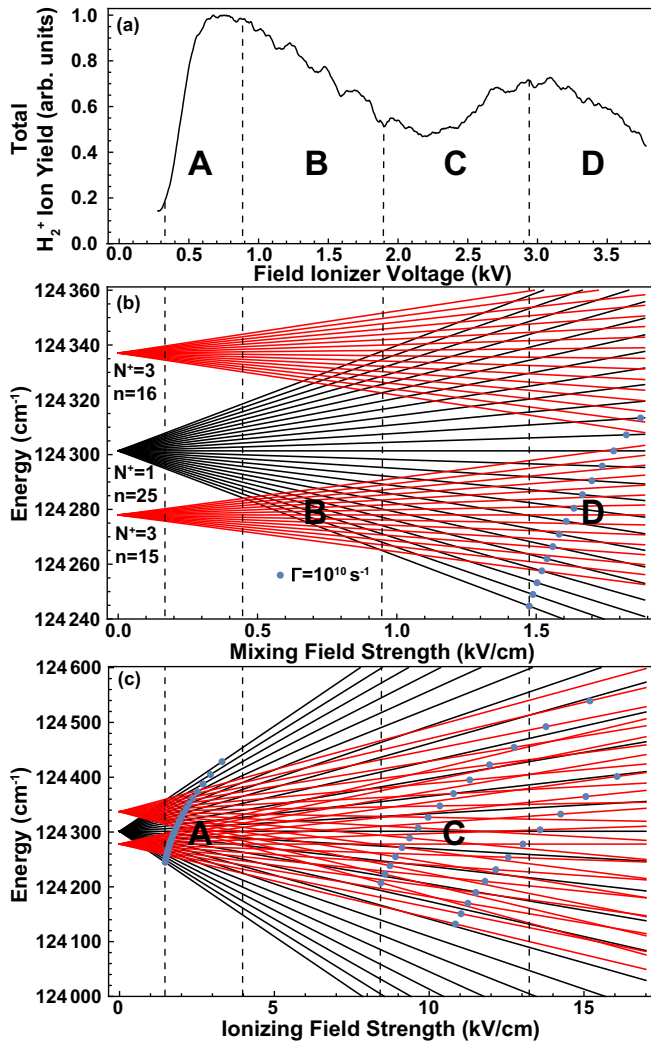


FIG. 9. Stark energy diagrams and field-ionization yield for $N^+ = 1, n = 25$. (a) Measured total field-ionization yield for excitation to $N^+ = 1, n = 25$. The hydrogenic ($m = 0$) $N^+ = 1, n = 25$ manifold (black) and the neighboring $N^+ = 3, n = 15$, and $n = 16$ manifolds (red) are shown for the mixing field (b) and ionizing field (c) for fields corresponding to the voltage on the center electrode of the field ionizer. The field, resulting in an ionization rate of $10^{10} s^{-1}$, is calculated for each Stark state by the ionization rate approximation for atomic hydrogen, as shown in Eq. (4) (blue dots).

requirements for $N^+ = 1$ (blue dots), and the ion yield increases until the entire $N^+ = 1$ manifold is ionized. In region B, the $N^+ = 1$ and $N^+ = 3$ manifolds cross and mix in the mixing field. The ionizing field ionizes $N^+ = 1$ but does not ionize $N^+ = 3$. Therefore, in this region, the total ion yield decreases as population is transferred from $N^+ = 1$ to $N^+ = 3$. In region C, the ionizing field now meets the ionization requirements for $N^+ = 3$ (blue dots) and, as a result, the total ion yield increases. Finally, in region D, the mixing field reaches the ionization requirements for $N^+ = 1, n = 25$ (blue

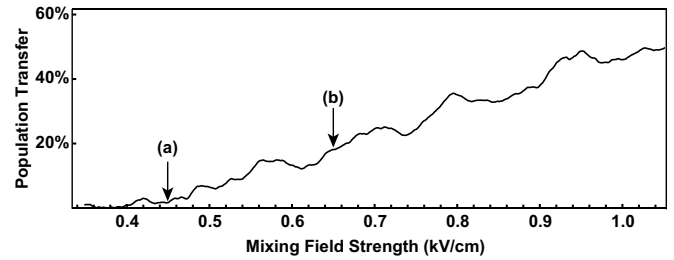


FIG. 10. Population transfer. The percentage of molecules mixed from $N^+ = 1, n = 25$ into neighboring $N^+ = 3$ manifolds is plotted as a function of field strength. The fields where Stark states of the $N^+ = 1, n = 25$ begin to cross Stark states of $N^+ = 3, n = 15$ (a) and $n = 16$ (b) are indicated with arrows.

dots). The resulting ions are not detected, leading to a decrease in the observed total ion yield, until the entire manifold has been ionized by the mixing field.

Subtracting the ionization yield in region B from the maximum ionization yield of region A allows for quantification of the population transfer from $N^+ = 1, n = 25$ into the neighboring $N^+ = 3$ manifolds. This is illustrated in Fig. 10 and indicates a large transfer of up to $\sim 50\%$ at high fields.

IV. SUMMARY

Field-ionized Rydberg states are isolated in kinetic energy from autoionizing states by two static fields. These static fields, in conjunction with a fast molecular Rydberg beam, result in a shaped pulse achieving field strengths up to $\sim 36 kV cm^{-1}$. The slew rate of the pulse is very high except at zero field and during the hold time of the mixing field. The experiment allows for manipulation of the pulse amplitude and therefore selectivity over the field strength at which mixing occurs in the Stark map. A total ionization yield is measured for molecules excited to $\nu = 0, N^+ = 1$ Rydberg states ($n = 17$ to 27).

The resulting yields are explained by Landau-Zener state mixing at the entrance and exit of field regions together with quantum time evolution in regions of constant field. Control over the rotational quantum state composition of the field-ionized molecules is demonstrated, showing population transfer of up to $\sim 50\%$ from $N^+ = 1$ to $N^+ = 3$. This experiment illustrates the potential usefulness of shaped pulses for the preparation of ions in selected quantum states.

ACKNOWLEDGMENTS

The authors thank D. Strickland and B. Strickland for their technical assistance at the Wesleyan machine shop and M. Koziol for electrical support. We also thank D. Jones, J. Dietz, and other undergraduate researchers for their work on the experimental setup. We acknowledge helpful conversations with S. Ashman, B. Stewart, M. Rosenberry, and L. Hüwel and support from T. Kottos, K. Setzer, and S. Shrestha.

[1] T. F. Gallagher, L. M. Humphrey, W. E. Cooke, R. M. Hill, and S. A. Edelstein, *Phys. Rev. A* **16**, 1098 (1977).

[2] F. G. Kellert, T. H. Jeys, G. B. McMillian, K. A. Smith, F. B. Dunning, and R. F. Stebbings, *Phys. Rev. A* **23**, 1127 (1981).

- [3] T. H. Jeys, G. W. Foltz, K. A. Smith, E. J. Beiting, F. G. Kellert, F. B. Dunning, and R. F. Stebbings, *Phys. Rev. Lett.* **44**, 390 (1980).
- [4] M. Tada, Y. Kishimoto, M. Shibata, K. Kominato, S. Yamada, T. Haseyama, I. Ogawa, H. Funahashi, K. Yamamoto, and S. Matsuki, *Phys. Lett. A* **303**, 285 (2002).
- [5] A. Gürtler and W. van der Zande, *Phys. Lett. A* **324**, 315 (2004).
- [6] H. Zhang, L. Wang, L. Zhang, C. Li, L. Xiao, J. Zhao, S. Jia, P. Cheinet, D. Comparat, and P. Pillet, *Phys. Rev. A* **87**, 033405 (2013).
- [7] R. Patel, N. J. A. Jones, and H. H. Fielding, *Phys. Rev. A* **76**, 043413 (2007).
- [8] C. R. Mahon, G. R. Janik, and T. F. Gallagher, *Phys. Rev. A* **41**, 3746 (1990).
- [9] M. A. O'Halloran, P. M. Dehmer, S. T. Pratt, J. L. Dehmer, and F. S. Tomkins, *J. Chem. Phys.* **90**, 930 (1989).
- [10] W. L. Glab and J. P. Hessler, *Phys. Rev. A* **42**, 5486 (1990).
- [11] E. Y. Xu, H. Helm, and R. Kachru, *Phys. Rev. A* **38**, 1666 (1988).
- [12] E. A. McCormack, M. S. Ford, and T. P. Softley, *J. Phys. Chem. A* **114**, 11175 (2010).
- [13] T. J. Morgan, C. F. Barnett, J. A. Ray, and A. Russek, *Phys. Rev. A* **20**, 1062 (1979).
- [14] H. A. Bethe and E. E. Salpeter, *Quantum Mechanics of One- and Two-Electron Atoms* (Springer, Berlin, 1957).
- [15] J. R. Rubbmark, M. M. Kash, M. G. Littman, and D. Kleppner, *Phys. Rev. A* **23**, 3107 (1981).
- [16] R. J. Damburg and V. V. Kolosov, *J. Phys. B* **12**, 2637 (1979).
- [17] W. J. Setzer, A. de Magalhaes, and T. J. Morgan, *J. Phys. Chem. A* **123**, 3535 (2019).
- [18] M. Menzinger and L. Wählin, *Rev. Sci. Instrum.* **40**, 102 (1969).
- [19] R. Kachru and H. Helm, *Phys. Rev. Lett.* **55**, 1575 (1985).
- [20] R. D. Knight and L.-g. Wang, *Phys. Rev. Lett.* **55**, 1571 (1985).
- [21] N. Bjerre, S. R. Keiding, L. J. Lembo, and H. Helm, *Phys. Rev. Lett.* **60**, 2465 (1988).
- [22] L. J. Lembo, N. Bjerre, D. L. Huestis, and H. Helm, *J. Chem. Phys.* **92**, 2219 (1990).
- [23] L. Dinu, Y. J. Picard, and W. J. v. d. Zande, *J. Chem. Phys.* **121**, 3058 (2004).
- [24] D. Sprecher, C. Jungen, and F. Merkt, *J. Phys. Chem. A* **117**, 9462 (2013).
- [25] V. I. Korobov, *Phys. Rev. A* **77**, 022509 (2008).
- [26] R. Moss, *Mol. Phys.* **80**, 1541 (1993).